ACS APPLIED MATERIALS & INTERFACES

Research Article

www.acsami.org

Triboelectrification Based Motion Sensor for Human-Machine Interfacing

Weiqing Yang,[†,‡,∥] Jun Chen,[†,∥] Xiaonan Wen,[†,∥] Qingshen Jing,[†] Jin Yang,[†] Yuanjie Su,[†] Guang Zhu,[†] Wenzuo Wu,[†] and Zhong Lin Wang*[,†,§]

[†]School of Materials Science and Engineering, Georgia Institute of Technology, Atlanta, Georgia 30332-0245, United States

[‡]Key Laboratory of Advanced Technologies of Materials (Ministry of Education), School of Materials Science and Engineering, Southwest Jiaotong University, Chengdu 610031, China

[§]Beijing Institute of Nanoenergy and Nanosystems, Chinese Academy of Sciences, Beijing, China

Supporting Information

ABSTRACT: We present triboelectrification based, flexible, reusable, and skin-friendly dry biopotential electrode arrays as motion sensors for tracking muscle motion and human−machine interfacing (HMI). The independently addressable, self-powered sensor arrays have been utilized to record the electric output signals as a mapping figure to accurately identify the degrees of freedom as well as directions and magnitude of muscle motions. A fast Fourier transform (FFT) technique was employed to analyse the frequency spectra of the obtained electric signals and thus to determine the motion angular velocities. Moreover, the motion sensor arrays produced a short-circuit current density up to 10.71 mA/m^2, and an open-circuit voltage as high as 42.6 V with a remarkable signal-to-noise ratio up to 1000, which enables the devices as sensors to accurately record and transform the motions of the human joints, such as elbow, knee, heel, and even fingers, and thus renders it a superior and unique invention in the field of HMI.

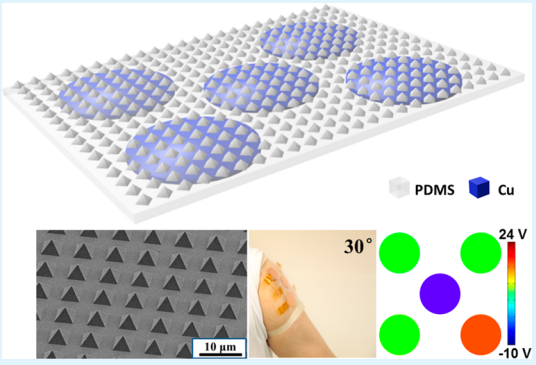

KEYWORDS: *triboelectrification, human−machine interfacing, self-powered, human joints, fast Fourier transform, motion sensor*

INTRODUCTION

Human−machine interfacing (HMI) is a method by which the user commands the robot to the desired state through biopotential monitoring system (BPMS),[1−4] which transforms body motions into electrical signals. Typically BPMS signal was acquired using wet electrodes,[5,6] in which Ag/AgCl is coupled to the skin via electrolyte gels and affixed with adhesive tapes or straps. Such a signal receiving system is a passive system that the electrodes are used only for signal transduction that is provided by the biosystem.

Recently, a triboelectric nanogenerator,[7−23] a coupling of the universally known contact electrification effect[24−29] and electrostatic induction, has been extensively utilized to successfully build up cost-effective and robust self-powered sensing systems with superior performance, including vibration sensor,[13] chemical nanosensors,[14,15] biosensor,[16] displacement vector sensor,[17] acceleration sensor,[18] pressure sensor,[19] wind vector sensor,[20] tactile sensor,[21] tracking sensor,[22] and acoustic sensor.[23] It is known that human skin can have electrostatic charges once it is in contact with a dielectric material, so that the potential produced by the charges is a measure of the contact between the material and the skin. Here, we present a flexible, reusable, and skin-friendly motion sensor for human−machine interfacing. Based on triboelectrification, the as-fabricated device, relying on dry biopotential electrodes, is capable of accurately acquiring the real-time motion information from human joints. The periodic change of contact areas between human skin and polydimethylsiloxane (PDMS) establishes electric potential difference, and thus brings into charge transfer between the copper electrode and the ground. Functioned as a self-powered human motion sensor, the entire device is consisted of an array of independently addressable units, which can record the electric output signals as a mapping figure to transmit the kinematic information on human joints. The motion sensor arrays produced an open-circuit voltage as high as 42.6 V with a remarkable signal-to-noise ratio (SNR) of higher than 1000, which guarantees the superior sensitivity and selectivity of the devices as sensors to accurately record and impart the motions of the human joints, such as elbow, knee, heel, even finger. Our study shows a possibility of utilizing triboelectrification based and self-powered motion sensor system for HMI.

RESULTS AND DISCUSSION

The self-powered motion sensor system is an array of five independent flexible dry biopotential electrodes, as schematically shown in Figure 1a. The PDMS films, patterned with

Received: February 10, 2014
Accepted: April 29, 2014

   dx.doi.org/10.1021/am500864t | ACS Appl. Mater. Interfaces XXXX, XXX, XXX−XXX

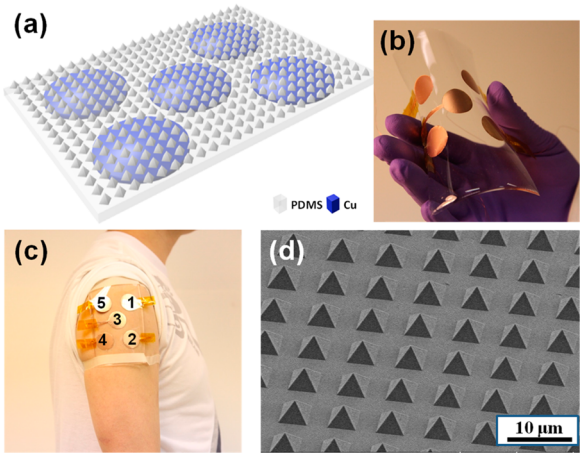

Figure 1. Triboelectrification based motion sensor for human–machine interfacing. A sketch (a) and photographs (b, c) of motion sensor array. (d) SEM image of the patterned PDMS film with pyramids features.

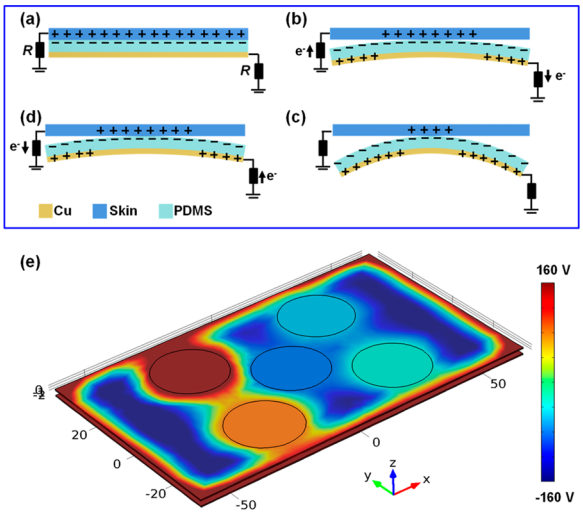

Figure 2. Sketch illustrating the working principle of the triboelectrification based motion sensors. (a) Original position of self-powered motion sensor. The positive and negative triboelectric charges are, respectively, generated on the human skin side and the PDMS side due to contact electrification. (b) The applied external force causes a partial separation and thus a gradually smaller contact area, screening the induced charges. (c) A position with minimum contact area between the two contact surfaces. (d) Electrons are driven back to the back electrode with the increasing of contact area. (e) Finite element simulation of the electric potential distribution. Note: The pyramid structure on the PDMS surface is not shown in the schematics for simplicity of illustration.

pyramid microstructure using a Si micropyramid template, were selected as the manufactured material due to its cleanability, skin-friendliness, light weight, good machinability and low cost. The photographs of an as-fabricated motion sensor array and its mounting on the surface of a shoulder joint are shown in Figure 1b and c, respectively. Figure 1d presents a scanning electron microscope (SEM) image of the micropatterned PDMS film, the surface of which is uniformly covered by orderly arrayed micropyramids with an edge length of about 4 μm. The corresponding thickness of the flexible PDMS film is about 1.0 mm. The as-designed micropyramid arrays play not only a role of spacer between the PDMS film and human skin, but also a role of a contact surface, which can induce a large triboelectric charge density due to the compressional deformation between human skin and PDMS. Moreover, the stretchable property of PDMS brings into a relative sliding between the two contact surfaces, the process of which is further illustrated in Supporting Information Figure S1. Additionally, by virtue of e-beam sputtering, copper was deposited onto the planar PDMS surface with circle diameters of 1.55 cm as back electrodes. A SEM image of copper coated PDMS surface is shown in Figure S2.

The working principle of the triboelectrification enabled motion sensor is schematically illustrated in Figure 2. In the original position, the full contact of human-skin and micropatterned PDMS surface brings into charge transfer between them due to the contact electrification. According to the triboelectric series,[30−32] electrons were injected from the human skin to the PDMS since PDMS is more triboelectrically negative than human skin. The generated triboelectric charges with opposite polarities stayed in a same plane and were fully balanced, resulting in no electron flow in the external circuit, as shown in Figure 2a. Once the partial separation between PDMS and human-skin occurs due to muscle motion, these triboelectric charges in insulative PDMS cannot be compensated and an electric potential difference is thus established, which drives free electrons to flow from the copper electrode to the ground, as shown in Figure 2b. When the separation area of the two contact surfaces increased to the maximum, the induced positive charges on the copper electrodes would also be maximized (Figure 2c). Subsequently, the separation area decreased (Figure 2d), and so did the induced positive charges of copper electrode. Electrons flow back to the copper electrodes from the ground until the skin and PDMS completely contact each other again, namely, back to the original position. This is a full cycle of the electricity generation process for the motion sensors. Moreover, to obtain a more quantitative understanding of the proposed working principle, finite element analysis were employed to theoretically study the electric potential distribution of the self-powered motion sensors, as shown in Figure 2e.

In order to identify the kinetic information (angles and angular velocities) of the shoulder joints, such as up-and-down, fore-and-aft swing as well as rolling motions of the upper arm, the as-fabricated motion sensor was mounted to a shoulder joint to record and transmit the kinetic signals to command the robot as well as exoskeletons. The corresponding $V-t$ and $I-t$ of the five independent local sensors depicted in Figure 1c are shown in Figure 3. The open-circuit voltages (V_{OC}) and short circuit currents (I_{SC}) signals of five sensor units were recorded when the shoulder joint moved up-and-down with the included angles θ in a range of from 0 to 90° in the sagittal plane. An illustrated definition of angle θ is presented in Supporting Information Figure S3. The open circuit voltages of five independent sensors are obviously different from each other, as demonstrated in Figure 3a, owning to the discrepancies of time-dependent change of the effective contact areas between PDMS and human skin in the course of arm up-and-down motion. The open-circuit voltages (V_{OC}) of sensors 1, 2, 3, 4, and 5 are respectively 2.9 (±0.4) V, 5.5 (±0.3) V, 22.9 (±1.4) V, 13.2 (±1.0) V, and 10.9 (±0.6) V. Among them, the highest voltage of sensor 3 is about 8 times larger than that of the lowest from sensor 1. In addition, as shown in Figure 3b (1−5), the short-circuit currents (I_{SC}) of sensors 1, 2, 3, 4, and 5 are 0.217 (±0.019) μA, 0.129 (±0.016) μA, 2.020 (±0.060) μA, 0.031 (±0.006) μA, and 0.012 (±0.001) μA, respectively.

dx.doi.org/10.1021/am500864t | ACS Appl. Mater. Interfaces XXXX, XXX, XXX−XXX

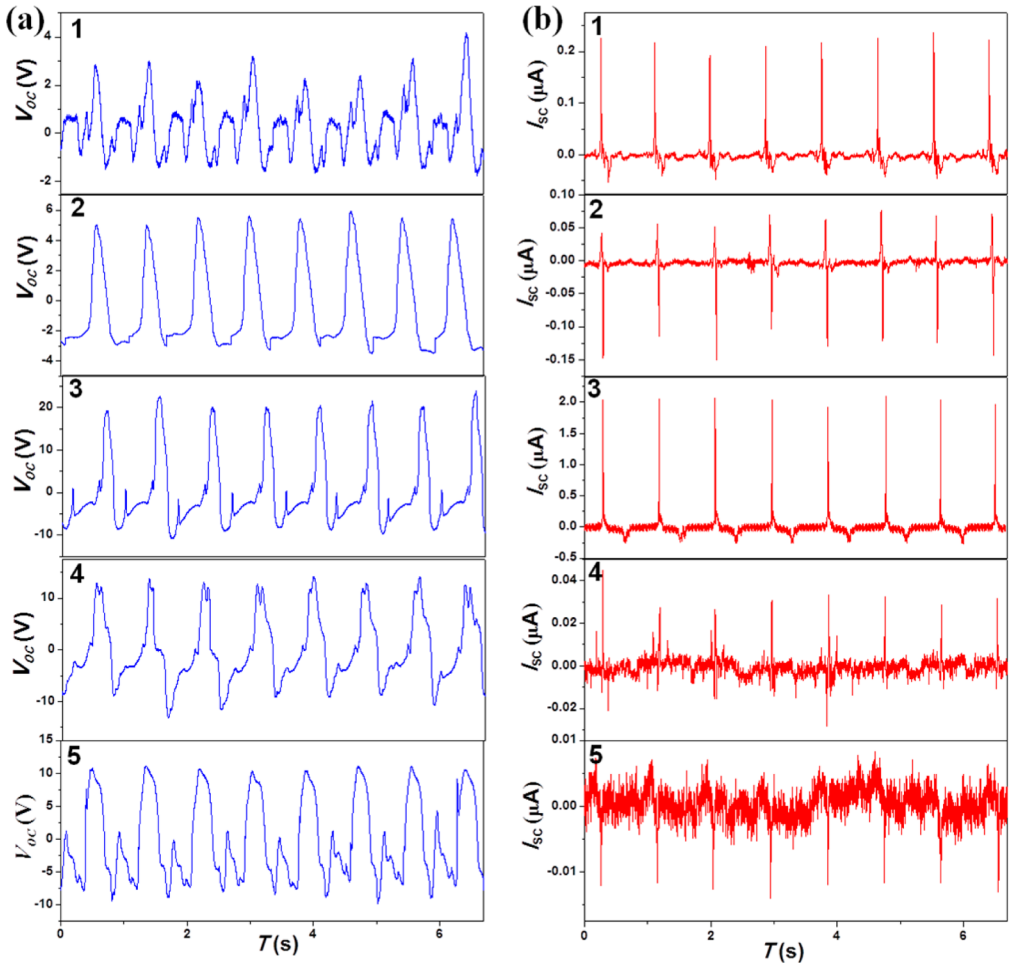

Figure 3. Electrical measurement results of the triboelectrification based motion sensors array, which was mounted on the human shoulder and undergoing an up-down motion of the upper arm. (a) Open-circuit voltages (*Voc*) of sensors 1−5. (b) Short-circuit currents (*Isc*) of sensors 1−5.

And the largest current value is about 168 times larger than the lowest value. Such a large difference is attributed to a distinctly larger separation distance of sensor 3 than all the others. Besides, as shown in Figure S4, the electric output of sensor 3 with pyramid-structure has about 2.01 times enhancement than that with planar PDMS surfaces. The surface pyramid nanostruature effectively enhanced the contact area between PDMS and human skin, and thus, a larger electric output is expected. In addition, we repeated same measurement five times on the same device to investigate its long-term stability, and the obtained results are rendered in Figure S5, which sufficiently proved the robustness and reusability of the as-fabricated devices as motion sensors.

The output voltages of five sensors units were simultaneously and independently recorded in real time as a mapping figure. As demonstrated in Figure 4, when the upper arm move upward (Figure 4a−e) and downward (Figure 4e−h), the voltage varied in a range of from −9 to 24 V, corresponding to the normal angles changed from 0 to 90° for the five sensors. It is worthwhile to note that not only the mapping figures of normal angles (θ) are quite different from each other, but also the mapping figures with fixed normal angle and different motion direction are different, indicating that not only the positions of the upper arm but also its motion direction can be identified by the mapping figures. Besides, to differentiate and identify each motion, FFT was utilized to analyze the output voltage signals

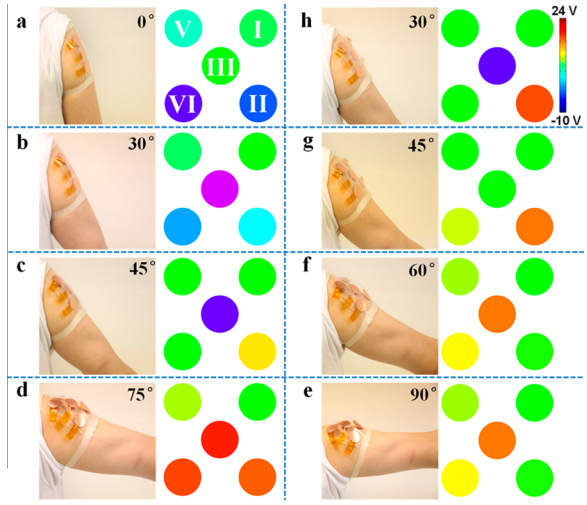

Figure 4. Electrical measurement results of the triboelectrification based motion sensors array when it was mounted on the human shoulder joints undergoing an up-down motion of upper arm. (a−h) Photographs and the corresponding measured output voltage mapping of a complete cycle of up-down motion (a−e, up motion and e−h, down motion).

of sensor 3 (Figure 5a), and the obtained FFT spectrum is shown in Figure 5b, from which we can read the fundamental frequency f_0 is 1.17 Hz and thus the average angular velocity of

dx.doi.org/10.1021/am500864t | ACS Appl. Mater. Interfaces XXXX, XXX, XXX−XXX

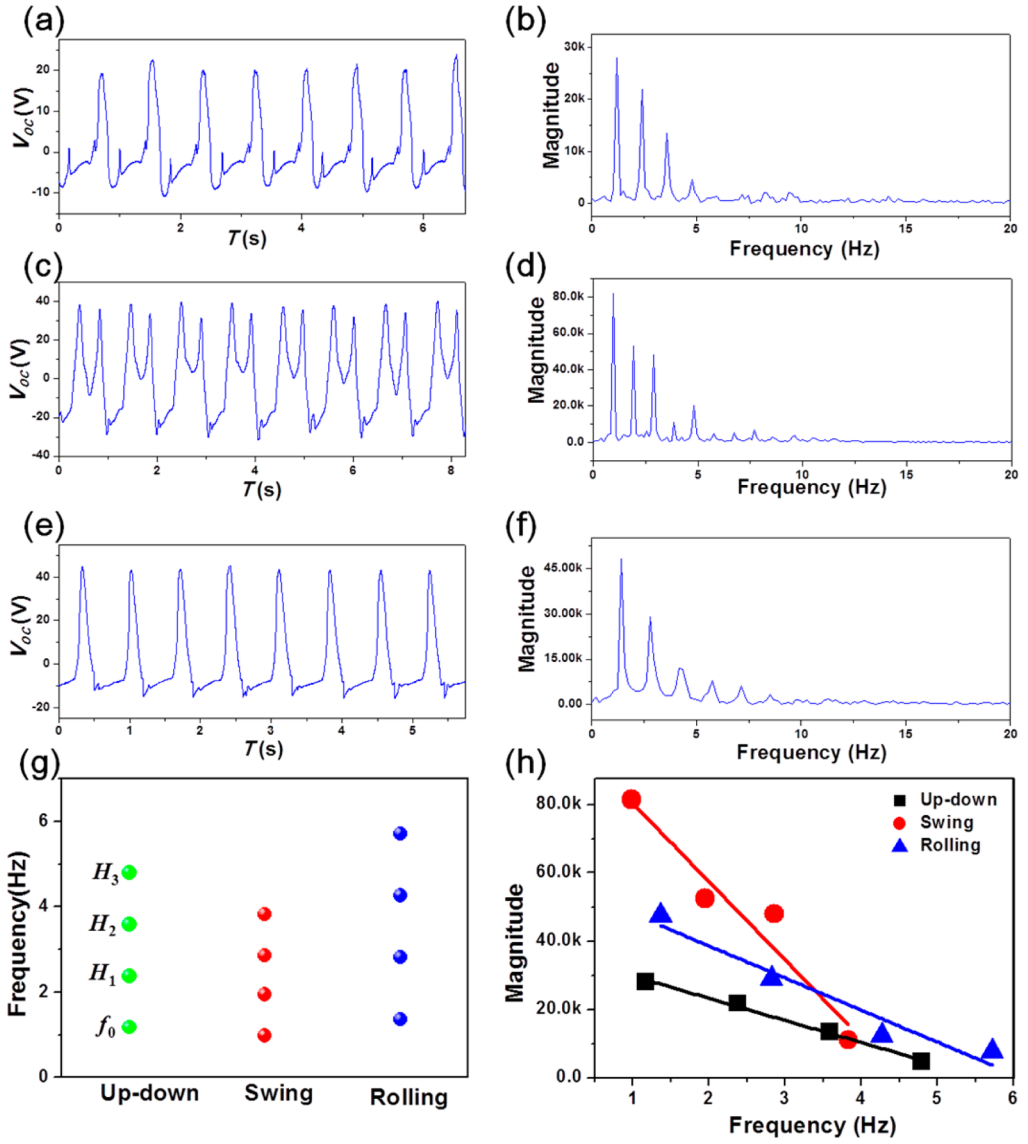

Figure 5. Electrical measurement results and the corresponding signal processing of triboelectrification based motion sensors array with mounting on a human shoulder joint. (a, c, e) The open-circuit voltages (V_{oc}) and their corresponding FFT (b, d, f) of sensor 3 in the course of up-down, swing, and rolling motion of upper arm, respectively. (g) One-dimensional digital signals and (h) two-dimensional digital signals of three motions.

the upper arm's up-and-down motion can be calculated as $\omega_1 = \pi f_0 \approx 3.68$ rad/s. Additionally, as shown in Figure 5 (c–f), the output voltage signals of the upper arm's swing (Figure 5c and d) and ring motions (Figure 5e and f) and their corresponding FFT frequency spectra can evidently identify the unique characteristic of each motion and thus well and truly transmit to command robotic or exoskeleton. And that the remarkable SNR of sensor 3 is more than 1000 (please see Supporting Information Figure S6), which guarantees the sensitivity and selectivity of the devices as sensors to accurately record and impart the motions of the human joints. Likewise, the average angular velocity of motions of swing at $\varphi = 3\pi/4$ and rolling at $\phi = 2\pi$ motions (please see Supporting Information Figure S3) can be easily calculated to be $\omega_2 = 3\pi 0.98/2 \approx 4.62$ rad/s and $\omega_3 = 2\pi 1.36 \approx 8.55$ rad/s. Furthermore, as shown in Figure 5g, the harmonic frequencies (H_1, H_2, H_3) of motions are an integral multiple of the corresponding fundamental frequencies (f_0), evidently justifying the typical harmonic motions. The obtained one dimensional digital signal can be provided to command the robot or exoskeleton. Meanwhile, Figure 5h presents the two dimensional digital signals of three motions, in which we can obtain the unique magnitude variations with a function of FFT harmonic frequency. And the slopes of corresponding fitting straight lines are −6475, −22 895, and −9389 per Hz for the up-down, swing, and rolling motion of the upper arm, respectively. Consequently, the real-time mapping figures of matrix sensors can record the motion angle and direction of the upper arms, and the corresponding FFT spectra of output voltage signals can be utilized to identify the angular velocities as well as motion modes.

Likewise, the short-circuit currents and their corresponding FFT frequency spectra of the upper arm's up-down, swing and rolling motions were also measured and demonstrated in Figure 6. These signals can also be used to identify the kinematics information (angles and angular velocities) of shoulder joints. Furthermore, as shown in Figure S7 and S8, reliance on the first differentials of output voltage signals and their corresponding FFT frequency spectra, more kinematic information can be extracted upon users' requirements. In addition, the motion sensors

dx.doi.org/10.1021/am500864t | ACS Appl. Mater. Interfaces XXXX, XXX, XXX−XXX

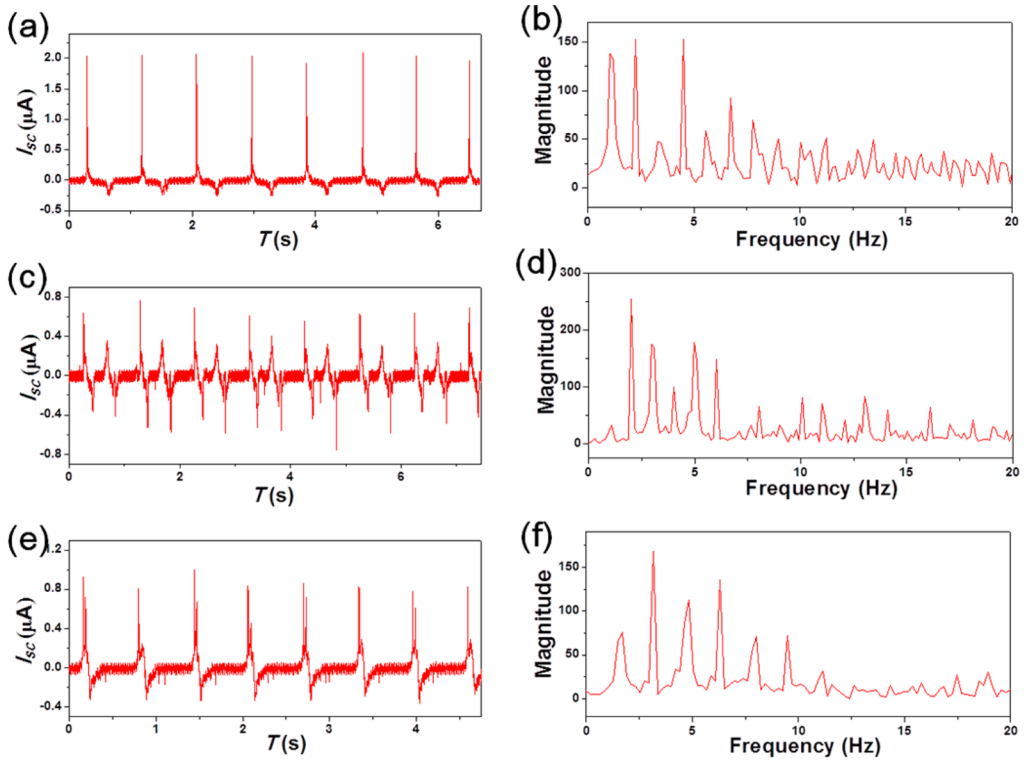

Figure 6. Signal processing of the short-circuit currents (I_{sc}) in the course of up-and-down, swing, and rolling motion. First differential (a, c, e) and corresponding FFT (b, d, f) of sensor 3 in the upper arm's up-down, swing, and rolling motion, respectively.

not only can record the motion information from shoulder joints to command the robot or exoskeleton (Supporting Information Movies 1 and 2), but also can be applied to other human joints, such as elbow joints (Supporting Information Figure S9, Movies 3 and 4) and knee joints (Supporting Information Figure S10, Movies 5 and 6), which obviously demonstrated the extensive applicability of recording and transforming human motions, and thus its great potential of attracting widespread attentions in the field of HMI.

CONCLUSIONS

We have developed a triboelectrification based, flexible, reusable, and skin-friendly dry biopotential electrode arrays as motion sensor for HMI. The independently addressable self-powered sensors array can record the electric output signals as a mapping figures to accurately identify the degrees of freedom as well as directions of human joints motion. The FFT frequency spectra of the obtained electric signals can be utilized to determine the motion angular velocities. Moreover, the motion sensors array produced a short-circuit current density up to 10.71 mA/m^2, and an open-circuit voltage as high as 42.6 V with a remarkable SNR up to 1000, which enables the devices as sensors to accurately record and transform the kinetic information on the human joints, such as elbow, knee, heel, even finger. This work has the potential toward the practical applications of a flexible dry biopotential electrode based self-powered motion sensor system for HMI.

ASSOCIATED CONTENT

Supporting Information

(1) Sketch that illustrates the impact induced inducing contact area increasing between human skin and PDMS film. (2) SEM image of Cu coated PDMS surface. (3) Sketch that illustrates the up-down, swing, and rolling motions of upper arm when a motion sensor was mounted at a human shoulder joint. (4) Electric output of motion sensors with and without pyramid-structured PDMS surface. (5) Investigation of the stability of motion sensors. (6) Signal-to-noise ratio estimation for the acquired voltage signal. (7) Signal processing of the open-circuit voltages (V_{oc}), which was acquired in the course of the up-down, swing and rolling motion of upper arm. (8) Comparisons of the open-circuit voltages (V_{oc}), which was acquired during the course of the human shoulder's up-and-down, swing, and rolling motion. (9) Electrical measurement results of the tribo-electrification based motion sensors array when it was mounted on the human elbow joints when undergoing the up-down motion of human arm. (10) Electrical measurement results of motion sensor arrays based TENG mounted on the human knee joints when the left-and-right swing. (11) Supporting movies. This material is available free of charge via the Internet at http://pubs.acs.org.

AUTHOR INFORMATION

Corresponding Author

*E-mail: zlwang@gatech.edu.

Author Contributions

[‖]W.Y., J.C., and X.W. contributed equally to this work. The manuscript was written through contributions of all authors. All authors have given approval to the final version of the manuscript.

Notes

Patents have been filed based on the research results presented in this manuscript.

The authors declare no competing financial interest.

■ ACKNOWLEDGMENTS

Research was supported by the U.S. Department of Energy, Office of Basic Energy Sciences (Award DE-FG02-07ER46394) and the "thousands talents" program for pioneer researcher and his innovation team, China, Beijing City Committee of science and technology project (Z131100006013004, Z131100006013005).

■ REFERENCES

(1) Mannsfeld, S. C. B.; Tee, B. C-K.; Stoltenberg, R. M.; Chen, C. V. H.; Barman, S.; Muir, B. V. O.; Sokolov, A. N.; Reese, C.; Bao, Z. N. Highly Sensitive Flexible Pressure Sensors with Microstructured Rubber Dielectric Layers. *Nat. Mater.* **2010**, *9*, 859−864.

(2) Schwartz, G.; Tee, B. C. K.; Mei, J. G.; Appleton, A. L.; Kim, D. H.; Wang, H. L.; Bao, Z. N. Flexible Polymer Transistors with High Pressure Sensitivity for Application in Electronic Skin and Health Monitoring. *Nat. Commun.* **2013**, *4*, 1859.

(3) Gong, S.; Schwalb, W.; Wang, Y. W.; Chen, Y.; Tang, Y.; Si, J.; Shirinzadeh, B.; Cheng, W. L. A Wearable and Highly Sensitive Pressure Sensor with Ultrathin Gold Nanowires. *Nat. Commun.* **2014**, *5*, 3132.

(4) Zhou, J.; Gu, Y. D.; Fei, Peng; Mai, W. J.; Gao, Y. F.; Yang, R. S.; Bao, G.; Wang, Z. L. Flexible Piezotronic Strain Sensor. *Nano Lett.* **2008**, *8*, 3035−3040.

(5) Webster, J. G. *Medical Instrumentation, Application and Design*; Wiley: New York, 1998.

(6) Jeong, J. W.; Yeo, W. H.; Akhtar, A.; Norton, J. J. S.; Kwack, Y. J.; Li, S.; Jung, S. Y.; Su, Y. W.; Lee, W.; Xia, J.; Cheng, H. Y.; Huang, Y. G.; Choi, W. S.; Bretl, T.; Rogers, J. A. Materials and Optimized Designs for Human-Machine Interfaces Via Epidermal Electronics. *Adv. Mater.* **2013**, *25*, 6839−6846.

(7) Zhu, G.; Chen, J.; Zhang, T.; Jing, Q.; Wang, Z. L. Radial-Arrayed Rotary Electrification for High Performance Triboelectric Generator. *Nat. Commun.* **2014**, *5*, 3426.

(8) Zhu, G.; Chen, J.; Liu, Y.; Bai, P.; Zhou, Y.; Jing, Q.; Pan, C.; Wang, Z. L. Linear-Grating Triboelectric Generator Based on Sliding Electrification. *Nano Lett.* **2013**, *13*, 2282−2289.

(9) Yang, W.; Chen, J.; Zhu, G.; Yang, J.; Bai, P.; Su, Y. J.; Jing, Q.; Cao, X.; Wang, Z. L. Harvesting Energy From the Natural Vibration of Human Walking. *ACS Nano* **2013**, *7*, 11317−11324.

(10) Yang, W.; Chen, J.; Zhu, G.; Wen, X. N.; Bai, P.; Su, Y. J.; Lin, Y.; Wang, Z. L. Harvesting Vibration Energy by a Triple-Cantilever Based Triboelectric Nanogenerator. *Nano Res.* **2013**, *6*, 880−886.

(11) Bai, P.; Zhu, G.; Liu, Y.; Chen, J.; Jing, Q.; Yang, W.; Ma, J. S.; Zhang, G.; Wang, Z. L. Cylindrical Rotating Triboelectric Nanogenerator. *ACS Nano* **2013**, *7*, 6361−6366.

(12) Yang, J.; Chen, J.; Yang, Y.; Zhang, H. L.; Yang, W.; Bai, P.; Su, Y. J.; Wang, Z. L. Broadband Vibration Energy Harvesting Based on Triboelectric Nanogenerator. *Adv. Energy Mater.* **2014**, *4*, 1301322.

(13) Chen, J.; Zhu, G.; Yang, W.; Jing, Q.; Bai, P.; Yang, Y.; Hou, T. C.; Wang, Z. L. Harmonic-Resonator-Based Triboelectric Nanogenerator as a Sustainable Power Source and a self-Powered Active Vibration Sensor. *Adv. Mater.* **2013**, *25*, 6094−6099.

(14) Lin, Z.H.; Zhu, G.; Zhou, Y. S.; Yang, Y.; Bai, P.; Chen, J.; Wang, Z. L. A Self-Powered Triboelectric Nanosensor for Mercury Ion Detection. *Angew. Chem. Int. Ed.* **2013**, *125*, 5169−5173.

(15) Zhang, H.; Yang, Y.; Su, Y.; Chen, J.; Hu, C.; Wu, Z.; Liu, Y.; Wong, C. P.; Bando, Y.; Wang, Z. L. Triboelectric Nanogenerator as Self-Powered Active Sensors for Detecting Liquid/Gaseous Water/Ethanol. *Nano Energy* **2013**, *2*, 693−701.

(16) Yang, Y.; Zhang, H.; Chen, J.; Lee, S.; Hou, T.C.; Wang, Z. L. Simultaneously Harvesting Mechanical and Chemical Energies by a Hybrid Cell for Self-Powered Biosensors and Personal Electronics. *Energy Environ. Sci.* **2013**, *6*, 1744−1749.

(17) Yang, Y.; Zhang, H.; Chen, J.; Jing, Q.; Zhou, Y. S.; Wen, X.; Wang, Z. L. Single-Electrode-Based Sliding Triboelectric Nanogenerator for Self-Powered Displacement Vector Sensor System. *ACS Nano* **2013**, *7*, 7342−7351.

(18) Zhang, H.; Yang, Y.; Su, Y.; Chen, J.; Adams, K.; Lee, S.; Hu, C.; Wang, Z. L. Triboelectric Nanogenerator for Harvesting Vibration Energy in Full Space and as Self-Powered Acceleration Sensor. *Adv. Funct. Mater.* **2014**, *24*, 1401−1407.

(19) Lin, L.; Xie, Y.; Wang, S.; Wu, W.; Niu, S.; Wen, X.; Wang, Z. L. Triboelectric Active Sensor Array for Self-Powered Static and Dynamic Pressure Detection and Tactile Imaging. *ACS Nano* **2013**, *7*, 8266−8274.

(20) Yang, Y.; Zhu, G.; Zhang, H.; Chen, J.; Zhong, X.; Lin, Z. H.; Su, Y.; Bai, P.; Wen, X.; Wang, Z. L. Triboelectric Nanogenerator for Harvesting Wind Energy and as Self-Powered Wind Vector Sensor System. *ACS Nano* **2013**, *7*, 9461−9468.

(21) Yang, Y.; Zhang, H.; Lin, Z.H.; Zhou, Y. S.; Jing, Q.; Su, Y.; Yang, J.; Chen, J.; Hu, C.; Wang, Z. L. Human Skin Based Triboelectric Nanogenerators for Harvesting Biomechanical Energy and as Self-Powered Active Tactile Sensor System. *ACS Nano* **2013**, *7*, 9213−9222.

(22) Su, Y.; Zhu, G.; Yang, W.; Yang, J.; Chen, J.; Jing, Q.; Wu, Z.; Jiang, Y.; Wang, Z. L. Triboelectric Sensor for Self-Powered Tracking of Object Motion inside Tubing. *ACS Nano* **2014**, *8*, 3843−3850.

(23) Yang, J.; Chen, J.; Liu, Y.; Yang, W.; Su, Y.; Wang, Z. L. Triboelectrification-Based Organic Film Nanogenerator for Acoustic Energy Harvesting and Self-Powered Active Acoustic Sensing. *ACS Nano* **2014**, *8*, 2649−2657.

(24) Lowell, J.; Roseinnes, A. C. Contact Electrification. *Adv. Phys.* **1980**, *29*, 947−1023.

(25) Castle, G. S. P. Contact Charging between Insulators. *J. Electrost.* **1997**, *40-1*, 13−20.

(26) Horn, R. G.; Smith, D. T. Contact Electrification and Adhesion Between Dissimilar Materials. *Science* **1992**, *256*, 362−364.

(27) Horn, R. G.; Smith, D. T.; Grabbe, A. Contact Electrification Induced by Monolayer Modification of A Surface and Relation to Acid-base Interactions. *Nature* **1993**, *366*, 442−443.

(28) Baytekin, H. T.; Patashinskii, A.I.; Branicki, M.; Baytekin, B.; Grzybowski, B.A. The Mosaic Surface Charge in Contact Electrification. *Science* **2011**, *333*, 308−312.

(29) Soh, S.; Kwok, S.W.; Liu, H.; Whitesides, G.M. Contact De-electrification of Electrostatically Charged Polymers. *J. Am. Chem. Soc.* **2012**, *134*, 20151−20159.

(30) Cross, J. A. *Electrostatics: Principles, Problems and Applications*; Adam Hilger: Bristol, 1987; Chapter 2.

(31) Nemeth, E.; Albrecht, V.; Schulert, G.; Simon, F. Polymer Tribo-electric Charging: Dependence on Thermodynamic Surface Properties and Relative Humity. *J. Electrost.* **2003**, *58*, 3−16.

(32) Diaz, A. F.; Felix-Navarrro, R. M. A Semi-quantitative Tribo-electric Series for Polymeric Materials: the Influence of Chemical Structure and Properties. *J. Electrost.* **2004**, *62*, 227−290.